

POLITECNICO DI TORINO
Repository ISTITUZIONALE

Development of a PHM system for electrically actuated brakes of a small passenger aircraft

Original

Development of a PHM system for electrically actuated brakes of a small passenger aircraft / De Martin, A., Achille, R., Bertolino, A.C., Jacazio, G., Sorli, M.. - 8 (1):(2024), pp. 337-348. (8th European Conference of the Prognostics and Health Management Society 2024 Prague (CZ) July 3rd - July 5th , 2024) [10.36001/phme.2024.v8i1.4002].

Availability:

This version is available at: 11583/2992738 since: 2024-09-24T12:18:19Z

Publisher:

PHM Society

Published

DOI:10.36001/phme.2024.v8i1.4002

Terms of use:

This article is made available under terms and conditions as specified in the corresponding bibliographic description in the repository

Publisher copyright

(Article begins on next page)

Development of a PHM system for electrically actuated brakes of a small-passenger aircraft

Riccardo Achille¹, Andrea De Martin², Antonio Carlo Bertolino³, Giovanni Jacazio⁴, and Massimo Sorli⁵

^{1,2,3,4,5}*Department of Mechanical and Aerospace Engineering, Politecnico di Torino, Torino, 10129, Italy*

riccardo.achille@polito.it

andrea.demartin@polito.it

antonio.bertolino@polito.it

giovanni.jacazio@formerfaculty.polito.it

massimo.sorli@polito.it

ABSTRACT

The evolution towards “more electric” aircraft has seen a decisive push in the last decade, due to the growing environmental concerns and the development of new market segments (Urban Air Mobility). Such push interested both the propulsion components and the aircraft systems, with the latter seeing a progressive trend in replacing the traditional solutions based on hydraulic power with electrical or electro-mechanical devices. Electro-mechanical brakes, or E-Brakes hereby onwards, would present several advantages over their hydraulic counterparts, mainly related to the avoidance of leakage issues and the simplification of the system architecture. Moreover, although it is expected a weight increase of the brake, the elimination of the hydraulic lanes would still come with an overall weight reduction. Despite these advantages, it remains a new, relatively unproven technology within the civil aviation field. Within this context, the development of PHM solutions would align with the need for an on-line monitoring of a relatively unproven component. This paper deals with the preliminary stages of the development of such PHM system for the E-Brake of a future executive class aircraft, iterating on previously published material and presenting a particle filtering approach based on a new degradation model and data provided through a revised high-fidelity model. The paper opens with the introduction to the research project and the technological demonstrator, positioning the performed work within the available literature. PHM activities, performed on simulated data-set are then presented and the preliminary results discussed.

Keywords: PHM, EMAs, Brakes, Particle filter.

Riccardo Achille et al. This is an open-access article distributed under the terms of the Creative Commons Attribution 3.0 United States License, which permits unrestricted use, distribution, and reproduction in any medium, provided the original author and source are credited.

1. INTRODUCTION

Electro-mechanical brakes, or E-Brakes, are the next step in the evolution of aeronautical braking systems, and the natural consequence of the push for the electrification of civil aviation which is strongly affecting the development of future platforms. E-Brakes have already found applications in civil aviation, with different architectures already flying on the latest iterations of the Boeing 787 and the Airbus A-220 and have drawn interest in the aeronautic community thanks to the significant advantages over their hydraulic counterpart, including lower weight, the elimination of long hydraulic pipelines and a lower environmental imprint. Despite these success stories, they remain a relatively unproven and more complex technology with respect to the traditional hydraulic solution. The definition of a comprehensive PHM system, leveraging the higher number of sensors usually employed on electro-mechanical system, would provide additional confidence towards their application, lowering the risk of unanticipated failures, reducing the aircraft downtimes and giving access to strategic information useful to optimize the fleet management. Although literature on PHM activities for the most common components of electro-mechanical brakes is extensive, few papers have been published about the E-Brakes themselves. In (Ramesh et al., 2021) authors propose a Fault Detection and Identification (FDI) algorithm to observe and correctly assess the most probable failures occurring in a simple electro-mechanical brake for aeronautic applications. The analysis considers an aeronautical brake actuated by one Electro-mechanical actuator driven through a brushed DC-motor and is mainly focused on electrical failures. In (Oikonomou et al., 2022) authors investigate the prognosis of wear in aeronautical brakes through the analysis of historical series of brake pads thickness. Data-driven techniques are applied to perform the long-term prognosis, and the results of an interesting benchmarking activities comparing the performances of several algorithms are provided. Results are promising but assume the presence of

dedicated sensors to measure the thickness of the brake pads, which are not foreseen for the application under study in this paper. The E-LISA research project, performed within the Clean Sky 2/Clean Aviation framework, has the objective of developing an innovative iron bird dedicated to executing tests on the landing gear of a small aircraft equipped with an electro-mechanical landing gear and electrical brake. The E-LISA iron bird consists of a multi-functional intelligent test facility integrating hardware and software, allowing all the tests and analyses perceived as fundamental to be performed to demonstrate the maturity of an electro-mechanical landing gear, hence paving the way for its implementation in a small passenger aircraft. Such tests include the simulation of complete landing procedures under different operating conditions such as runway friction (wet/dry), presence of waving and irregularities along the runway, variable aircraft weight, and approach speed. At the same time, the rig will act as a technological demonstrator for PHM routines devoted to the analysis of the E-Brake health status. This paper opens with the description of the case study under analysis, a fully electrical landing gear leg for a new executive-class aircraft, detailing the system characteristics. Then the architecture of the technological demonstrator is presented, highlighting its most prominent features and the solutions required to meet its functional requirements. The focus is then shifted towards the definition of the PHM routines, where a possible scheme to detect and prognose the wear of the brake pads is proposed. A first-tentative approach to the problem was presented by authors in (De Martin, Jacazio, Parisi, et al., 2022), making use of a first-trial high-fidelity model and a simplified particle filtering approach. This study was used as a basis: the model was further evolved to take into consideration the effects of different combination of environmental conditions and tires types, while the prognostic algorithm was substantially modified considering a physics-based representation of the fault progression. Early results are presented, alongside a test-plan to support the simulation findings through experimental activities, once the rig is operational.

2. CASE STUDY

The case study under analysis is an E-Brake system for an executive-class aircraft with an expected weight at take-off ranging between 5.5 and 6.1 tons, depending on the passengers' number and the amount of unspent fuel. Two E-Brake systems are integral with the Main Landing Gear system, one for the Left-Hand side, one for the Right-Side each. Depicted in Figure 1, each E-Brake is a multi-disk assembly actuated through four Electro-Mechanical Actuators (EMAs) controlled in force. Whenever the pilot acts on the brake pedals, a force command is sent towards the E-Brake system; such command signal is processed by the Brakes Control Unit (BCU), which can cut the force command signal through the touch-down protection routines, avoiding that the brakes are actuated before the aircraft rotation during landing has ended. The command signal can

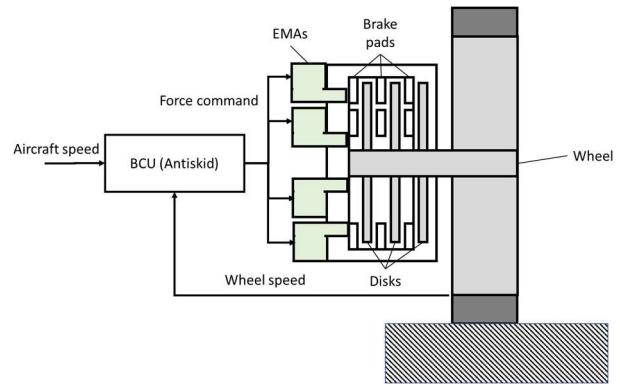


Figure 1. Case-study architecture.

be further modulated by the electronic anti-skid system, which decreases the force request depending on the runway conditions to avoid the occurrence of wheel blockage events and excessive slip according to a combination of pilot input and automatic recognition of the runway status. The electro-mechanical actuators are driven by one Brushless-DC motor with each, and act on the brake pads through a mechanical transmission made of a one-stage reducer and a ball-screw. Each actuator is equipped with a force sensor to measure the exerted action, while a resolver integral with the motor shaft is used to infer its position and realize the Field Oriented Control of its phase currents. The test-rig has been designed to exchange information with the E-Brake during its operations interfacing with the BCU. As such all the signals provided by the sensors employed in each EMAs are acquired and can be used for PHM. Such signals include the angular position of the E-Brake motors shaft, the braking command issued by the pilot, the anti-skid and touch-down protection signals and the exerted force measurement for each EMA. The phase currents of each electric motor are acquired as well, along with the current request provided by the force control loops.

3. THE TECHNOLOGICAL DEMONSTRATOR

The main purposes of the technological demonstrator are to support the testing and certification of a novel E-Brake system and to foster the definition of dedicated prognostic logic. As such, the main functional requirements are twofold. On one side it is paramount to be able to conduct the tests prescribed by the normative, such as the on-ground start-stop test and the landing procedure. On the other side, it is important to recreate on the test bench the widest array of operating conditions to stress as much as possible the PHM routines and provide statistically representative datasets. To achieve this goal the test rig is designed to allow the arbitrary variation of several operating parameters, including the aircraft approach speed, the dynamic load applied on the landing gear leg, the friction coefficient between the aircraft wheels and the runway and the occurrence of a selected number of electrical failure or mechanical faults. The architecture of the test rig is depicted in Figure 2, while a

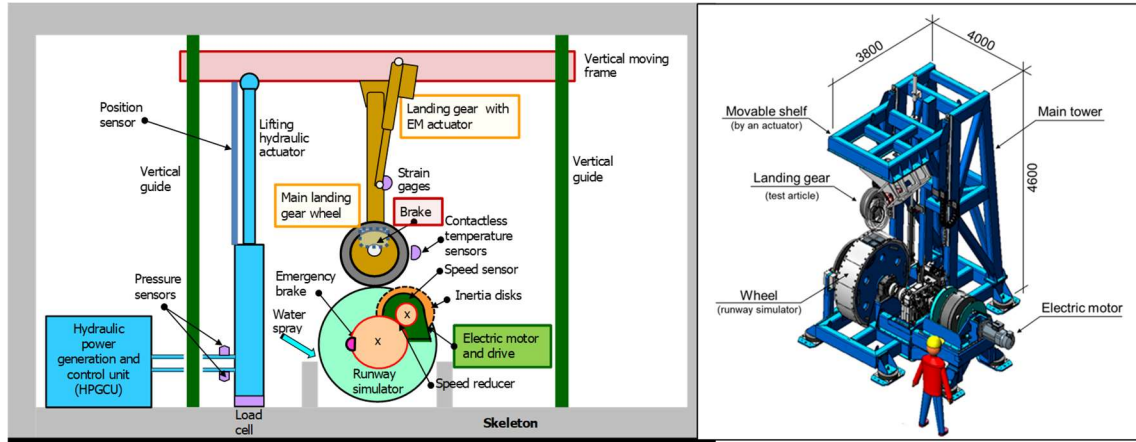


Figure 2. Iron bird schematics.

details of its mechanical structure can be retrieved in (Giannella et al., 2022). The mechanical structure can be divided between a fixed part and a moving platform integral with the landing gear leg, complete with a wheel and electrical brake. The moving platform can translate vertically along low friction guides according to the force provided by an electro-hydraulic servoactuator controlled through a 160 l/min servovalve. A calibrated by-pass orifice connects the two hydraulic lines serving the actuator to improve the dynamic response of the force-controlled system. The test-rig behavior is continuously monitored through one linear variable differential transformer (LVDT) sensor measuring the hydraulic actuator travel, a load cell measuring the force exchanged between the actuator and the moving platform and a differential pressure transducer sensing the pressure drop across the two actuator’s chambers. The hydraulic power available for the test-rig operation is that of the facilities in which the rig will be installed and is limited at 207 bar. The contact between the landing gear wheel and the runway is represented through a runway simulator, a rotating disk, connected to a selected number of inertia disks, representative of the aircraft inertia, through a gearbox. A different solution, based on a novel hydraulic system, was considered in (De Martin, Jacazio, Ruffinatto, et al., 2022) but discarded due to budget constraints. The diameter of the rotating cylinder is such to be representative of the expected linear speed of the aircraft along the runway during the landing procedure and must be higher than the wheel diameter to reduce at a minimum the differences between the wheel/runway simulator contact and the wheel/real runway contact. A gearbox is interposed to significantly reduce the mass and the encumbrance of the flywheels, the number of which can be increased or decreased to scale-up or scale-down the weight of the simulated aircraft. The runway simulator was designed with the possibility to change the external coating. To achieve the variation of the friction forces between the wheel and the runway and allow the verification of the anti-skid logic behavior in different operating conditions, while a sprinkler can be activated to

reproduce the wet-runway conditions. An electric motor is used to accelerate the runway simulator up to the angular frequency corresponding to the aircraft horizontal speed given the diameter of the rotating disk, while an emergency brake is installed in-line with the rotating cylinder, allowing to bring the full system to a complete stop in less than 60 s. The technological demonstrator is controlled through an engineering test station (ETS), which accepts the inputs from a central control unit (CCU) that in turn receives the commands from an operator via a user interface. The input signals are then sent together with rig measurements to a dedicated computer running a real-time (RT) representation of the aircraft dynamics during landing. Such real-time model is then used, along with a model of the runway and a model of the landing gear dynamics, to compute in real-time the load that must be applied to the test-article. The ETS also include the rig control logic, which is designed to manage both the position of the moving platform and the force exerted by the hydraulic actuator and include a safety routine check to limit the damages to the rig and to the test article in case of a failure of the anti-skid system during the execution of a test. The structure of the control system is depicted in Figure 3, where three main modules can be identified. The Simulation Module involves the real-time representation of the landing dynamics, including a real-time representation of the aircraft dynamics, a runway model, which allows to describe the presence of periodical or localized runway irregularities, and the model of the landing gear legs, each modelled as a two-degrees of freedom vibrating systems, where the mechanical

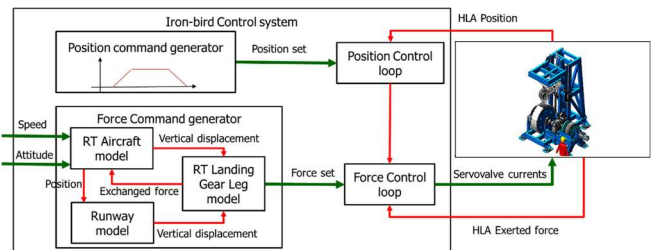


Figure 3. Control system structure.

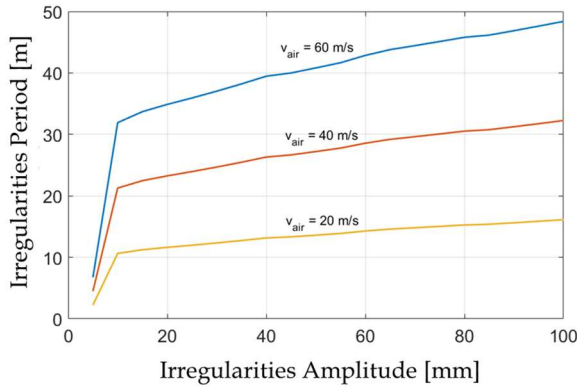


Figure 4. Projected limits on the representation of the periodical runway irregularities on the test-rig.

characteristics of the shock-absorber, of the tires and of the mechanical structure are provided by the industrial partners of the project. The control system is based on two control loops, one operating in position and the other on force, alternatively active before and after the contact between the landing gear wheel and the runway simulator. The control system, best described in (Bertolino et al., 2023) is designed to achieve bandwidth higher than 10 Hz in both force and position control loops. As shown in Figure 4, the control system, combined with the Real-Time simulation of the aircraft behavior during landing, it allows to reproduce on the test-rig the effects of periodical runway irregularities up to 100 mm depending on their period, the aircraft mass and its expected approach speed (De Martin, Jacazio, & Sorli, 2022).

4. SIMULATION ACTIVITIES

To achieve the definition of a PHM scheme for the entire E-Brake assembly a number of tasks are required. In order, there is the need to orderly assess which failure modes or which cause of service disruption to investigate, to prepare a high-fidelity model of the system representative of its operational performances and finally proceed to support such activities through experimental tests and validation. As stated in the introduction the technological demonstrator is not yet in function, thus the analysis is so far limited to simulation results. The failure modes being investigated includes the occurrence of several types of short circuits within the windings of the electro-mechanical actuators and wear of the mechanical transmission. Such failure modes, although important, are fairly common in electro-mechanical actuators independently from their function. As such, priority was given to the detection and prognosis of the wear of the brake pads. Although not a failure-mode per se, the reduction of the brake pad thickness is accompanied with a lower dynamic response of the brake and requires periodical maintenance operations. Currently wear of the brake pads is detected through dedicated sensors or through periodical inspection of

visual indicator on top of the brake itself. Making the monitor of the brake pads wear part of the PHM system would allow to limit or avoid the necessity of periodical inspections, anticipate the maintenance action and avoid unpredicted aircraft-on-ground situations. Authors started analyzing the possibility of such a system in (De Martin, Jacazio, Parisi, et al., 2022) through a simple particle filtering routine based on data coming from streamlined landing simulations. As more data were made available the analysis was improved through the definition of a higher-fidelity simulation model and a more realistic operational scenario. The prognostic routine was similarly revised and will be presented in the next sections of the paper.

4.1. System modelling

The high-fidelity simulation model includes a two-dimensional representation of the aircraft dynamics during landing, a three degrees-of-freedom multi-body model of the landing gear legs and of their interaction with the runway, and an in-detail representation of the E-Brake dynamics. Parts of such model, with particular reference to the aircraft dynamics and the vertical displacement of the landing gear leg were already described in (De Martin, Jacazio, & Sorli, 2022; De Martin, Jacazio, Parisi, et al., 2022) and won't be reported here, limiting the description to the component interested by modifications. Starting with the rotational dynamics of the wheel and addressing with $F_n = k_t(x_w - x_{rw}) + c_t(\dot{x}_w - \dot{x}_{rw})$ the vertical force exchanged between the wheel and the runway it is possible to express the wheel angular acceleration $\ddot{\vartheta}_w$ as a function of the rolling friction coefficient u_{rw} , expressed as a function of the wheel angular frequency and of the tire pressure (Carbone & Putignano, 2013), of the the moment of inertia of the wheel assembly I_w , the wheel diameter D_w and the viscous friction coefficient roughly representative of the dissipation in the wheel supports c_w .

$$F_n \mu \left[\frac{D_w}{2} - (x_{leg} - x_{rw}) \right] \text{sign}(\lambda) - F_n u_{rw} \tanh \dot{\vartheta}_w - c_w \dot{\vartheta}_w - T_{brk} = I_w \ddot{\vartheta}_w \quad (1)$$

The friction coefficient μ is evaluated according to a modified version of the Burckhardt model (M. Burckhardt, 1993), as a function of the slip factor λ between wheel and runway simulator and of the experimental parameters β_1, β_2 function of the tires temperature, thread type and runway conditions.

$$\mu(\lambda) = [\beta_1(1 - e^{-\beta_2\lambda}) - \beta_3\lambda] \mu_{max}(p_{tire}, v_{air}) \quad (2)$$

The parameter $\mu_{max}(p_{tire}, v_{air})$ is function of the tires pressure and of the aircraft speed and was fitted on experimental dataset provided for different combination of thread type and runway conditions for an aircraft of similar size to the target platform. An example of the fitter profiles is shown in Figure 5, where data for smooth tires on dry-runway

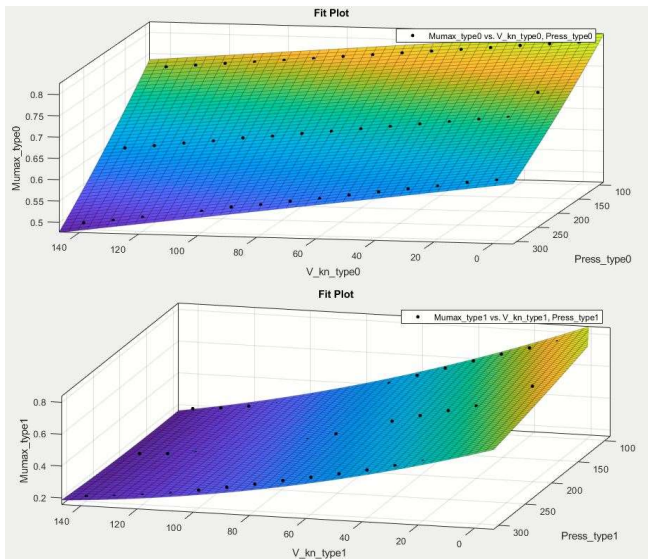


Figure 5. μ_{max} values for dry (above) and wet (below) runway conditions.

conditions are compared against data for threaded tires on a wet runway. The four Electro-Mechanical Actuators (EMAs) responsible for the braking action are controlled in force and act in parallel on the multi-disk brake. The control system is described as a two-nested control loops, where a sequence of Proportional-Integrative controllers operates on the force control loop and on the current control loop of each brushless motor. The sensors are modelled through second order transfer functions replicating the expected dynamics of the load cell and of the Hall-effect sensors employed to monitor the angular position of the Brushless-DC rotor. The simulation of the measure chain is complete with the model of the employed A/D converters. The dynamic model of each EMA features a functional description of the Electronic Power Converter derived from (Mohan et al., 2005) for a three-phase inverter controlled through Pulse Width Modulation (PWM). The electrical dynamics of the motor is described according to a streamlined three-phase model of the system, where $V_{a,b,c}$ and $i_{a,b,c}$ are the phase voltages and currents.

$$\begin{aligned} [V_{a,b,c}] &= [R_{a,b,c}(T_w)][i_{a,b,c}] + \\ [L(T_w)] \frac{d}{dt} [i_{a,b,c}] &+ \frac{d}{dt} [\phi_{a,b,c}(\vartheta_{el})] \end{aligned} \quad (3)$$

$[R_{a,b,c}]$ is the electric resistance matrix, which elements depends on the windings' temperature (T_w). The diagonal elements of the matrix represent the single-phase resistance, while the non-diagonal terms represent the electrical resistance provided by the insulating material separating the coils of different phases, addressed as phase-to-phase resistances hereafter. Such values can be degraded to simulate the effects of a turn-to-turn or phase-to-phase short respectively. $[L]$ is the inductance matrix, accounting for self-induction and mutual induction phenomena along with

the effect of magnetic flux dispersion. Finally, $[\phi_{a,b,c}]$ is the concatenated magnetic flux provided by the permanent magnets, function of the electrical angle (ϑ_{el}). The torque at the motor shaft can then be computed, leading to the dynamic equilibrium of the rotor

$$\begin{aligned} \sum_{a,b,c} \frac{d\phi}{dt} i_{a,b,c} - c\dot{\vartheta}_m - k_m(\vartheta_m - \vartheta_{gb}) \\ - c_m(\dot{\vartheta}_m - \dot{\vartheta}_{gb}) = I_m \ddot{\vartheta}_m \end{aligned} \quad (4)$$

where ϑ_m and ϑ_{gb} are the angular position of the motor shaft and of the gears. I_m is the moment of inertia of the rotor, while k_m and c_m address the torsional stiffness of the motor shaft and its associated damping. The gear pair is described as a rotational mass-spring-damper system, thus leading to the following equation,

$$\begin{aligned} k_m(\vartheta_m - \vartheta_{gb}) + c_m(\dot{\vartheta}_m - \dot{\vartheta}_{gb}) \\ - \frac{1}{\tau} [k_{gb}(\vartheta_{gb} - \vartheta_{rs}) + c_{gb}(\dot{\vartheta}_{gb} - \dot{\vartheta}_{rs})] - T_{fr,gb} \\ = I_{gb} \ddot{\vartheta}_{gb} \end{aligned} \quad (5)$$

where τ is the transmission ratio, $T_{fr,gb}$ the friction torque, while ϑ_{rs} is the angular position of the rotating part of the screw. The friction torque is computed as the sum of three components, one dependent on the acting load, one related to the viscous friction and a drag torque component. The power-screw is modelled as a two-degrees of freedom elements, where the rotating part is connected to the translating element through a viscoelastic element. Defining with $x_{rs,i}$ the position of the translating portion of the screw pertaining to the i -th actuator, it becomes possible to describe the brake dynamics, and thus that of the pads. Addressing with k_{eb} the stiffness, it is possible to evaluate the braking torque acting on the landing gear wheel as a function of the translating mass of the brake pads m_{eb} , its translation x_{eb} and the angular speed of the wheel $\dot{\vartheta}_w$ as,

$$\begin{cases} T_{brk} = 0 & \leftrightarrow x_{eb} < x_{thr} \\ T_{brk} = R_{eb} f_{eb} [k_{eb}(x_{eb} - x_{thr}) - c_{eb}(\dot{x}_{eb})] & x_{eb} \geq x_{thr} \end{cases} \quad (6)$$

where $f_{eb} = f_{eb}(\dot{\vartheta}_w)$ is the friction coefficient between the brake pads and disk, function of the wheel angular frequency. Knowing the braking torque and the wheel angular frequency it is possible to compute the mechanical power transformed into heat by the braking process. Such power is used within a simplified thermal model of the E-Brake assembly to estimate at each time step the temperature of the pads and the temperature of the electric motor windings considering both the thermal power generated by the motor themselves and that transmitted to the external environment. Since the pads contact the brake disks only when their translation x_{eb} overcomes a predefined stroke equal to x_{thr} , it is possible to model the effects of the pads wear by properly increasing such threshold value under the assumption that the brake pads return in the original position once the braking procedure is

finished. According to (Olesiak et al., 1997; Yevtushenko et al., 2017), wear progression in brake pads can be described as dependent on an experimental coefficient f_{wear} and k_{wear} , function of the local absolute temperature T , the sliding velocity between disks and pads v , and the contact pressure p . The dependency of the friction and wear coefficient on temperature is due to how the interaction between the disc and the brake pads occurs at a microscopic level. The brake performance (and its wear) depends on how the material of the pads bonds with the material of the disk and with the particles of the pads material which have remained bonded with the disc due to the run-in process and previous usage. This process is temperature dependent: at very-low temperature (-40°C) friction tends to increase in mechanical systems. Similar effects occurs at very high temperatures, where the bonding effects can be favored by localized fusion processes, accelerating the wear rate.

$$\Delta x_{thr} = \int_t f_{wear}(T)K_{wear}(T)v(t)p(t)dt \quad (7)$$

Expressing the sliding velocity as a function of the wheel angular frequency $\dot{\vartheta}_w$ and the radial coordinate of the pads with respect to the wheel axis R_{pad} , we have

$$v = \dot{\vartheta}_w R_{pad} \quad (8)$$

The average pressure within the pads/disks contact area can be computed as a function of the braking force exerted by the four actuators and the pad contact area.

$$p = \frac{k_{eb}(x_{eb} - x_{thr}) - c_{eb}(\dot{x}_{eb})}{A_{pad}} \quad (9)$$

An example of the model response is provided in Figure 6, where the system behavior in response to an emergency brake in presence of a wet runway and smooth tires is presented.

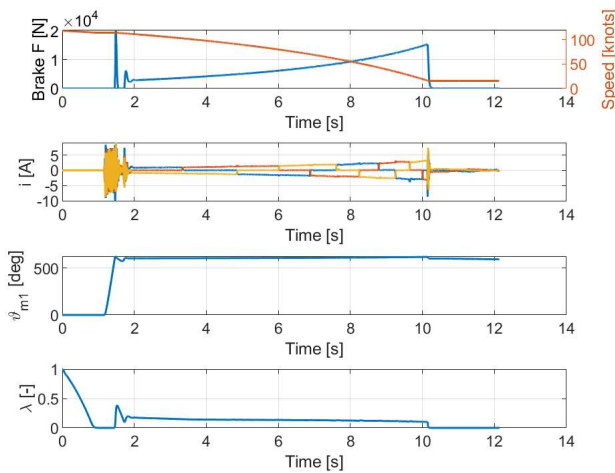


Figure 6. Example of the model response.

The figures depict the behavior of the total braking force expressed by the four EMAs, the aircraft speed along the runway, the three phase currents of the BLDC motor belonging to one of the EMAs (i [A]), the correspondent angular rotation of the motor shaft ϑ_{m1} and the slip factor λ between the wheel and the runway.

4.2. Operational scenario and data-base building

The simulation model is built for two main reasons: to generate a data-base to train and stress the PHM routines and to help in characterizing the system and provide additional information that could be useful to the PHM system itself. The first task in generating a reliable operational scenario is to characterize all possible sources of uncertainty of the system behavior. For the case study under analysis the following sources were identified and addressed.

- Aircraft mass at landing
- Runway temperature and conditions
- Tires type (smooth, threaded) and pressure
- Aircraft horizontal approach speed
- Type of braking procedure (emergency, normal)
- Production tolerances in the E-Brake system
- Pilot reaction time
- Sensors noise, deviations

The aircraft mass at landing is drawn randomly at each simulation from a uniform distribution ranging between 5.5 and 6.1 tons approximately, which is considered the expected variance depending on the passengers number, payload presence and type, and the remaining fuel. Runway temperature and conditions were taken into account by considering the temperature and rainfall distribution of three distinct area, each representative of a prevalently cold (Vancouver), hot (Dubai) and temperate (Rome) operating conditions. Data were obtained through public access database and randomly drawn at each simulation. Tires type is chosen at each simulation between threaded and smooth, while their pressure is randomly chosen from a normal distribution with mean 200 psi and variance 30 psi. The aircraft horizontal approach speed is randomly drawn from a normal distribution with mean equal to 110 knots and standard distribution equal to 5 knots. The type of braking procedure (whether emergency or normal) is decided before launching the simulation: during emergency stops, the pilot commands the E-Brake to supply its maximum force, while the anti-skid routine modulates such request to achieve the slip factor associated with the maximum friction coefficient between wheel and runway. On the contrary, during normal operations, the pilot modulates the braking force command trying to mimic a sequence of aircraft horizontal speed drawn from a pool of experimental results provided by the industrial partners of the project for an aircraft of similar size. An example of the difference between the two braking procedures is provided in Figure 7.

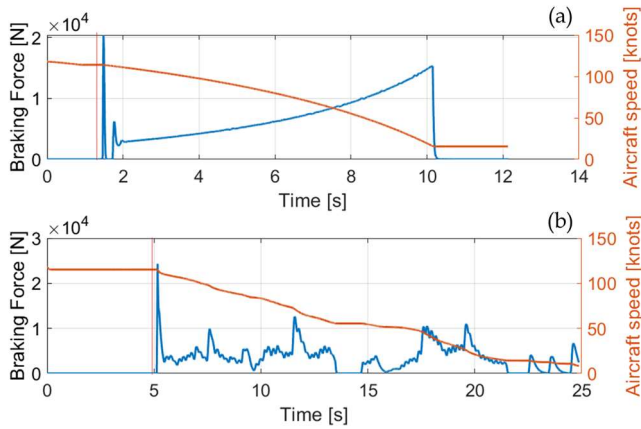


Figure 7. Comparison between emergency stop (a) and normal braking (b).

In this comparison, both aircrafts are decelerated down to 16 knots, which is the limit taxiing speed on most civil runways. Another uncertainty source related to the brakes performances is the pilot reaction time, which is modelled as a simple transport delay with time constant variable between 0.1 and 0.5 s.

These first uncertainty sources are expected to be the most significant for the E-Brake performances.

The aircraft speed and its mass at landing affects the overall kinetic energy to be dissipated through the brakes, while the operating conditions, tires type and inflating pressure affects the efficiency with which the braking torque produced by the electro-mechanical device is transferred to the ground.

Additional uncertainty sources, affecting the signals pertaining the E-Brake that can potentially be used for PHM includes the production tolerances, which were over imposed onto the main electrical and mechanical parameters of the EMAs, and sensors noise, modelled according to the indication provided in the manufacturer catalogues.

5. PHM ALGORITHM

The PHM algorithm for the wear of the brake pads is based upon the scheme presented in Figure 8, designed to leverage the physical knowledge of the system and employ the past knowledge of the E-Brake operations to better characterize the uncertainty distribution.

Prognosis is achieved through a Bayesian estimation method using a particle filtering approach, which provides after each landing an estimate of the current level of wear in the brake pads leveraging the indirect knowledge of the terms employed in the wear function provided in Equation 7. This step, functionally part of the fault identification process, is necessary to achieve the long term prognosis through physics-driven equations by supplying the particle filter with pdfs of future usage of the brake based on previous information retrieved and stored after each landing. Particle filters, firstly introduced in PHM by (Orchard & Vachtsevanos, 2009), take advantage of a nonlinear process (fault / degradation) model to describe the expected dynamics of the fault progression and a measure model derived from the feature/wear progression dependence observed during the feature selection phase. The particle filtering approach was chosen over other considered options (LSTMs in particular, were considered following previous works on a different application (Grosso et al., 2020)) for several reasons. The main one is that this process enables the estimation of the fault size through physics-based equations; since activities have been performed over simulated data-set, the adoption of a physics-driven approach was preferred to mitigate the risk of not operating on experimental datasets. The second reason is that brake pads wear is only one of the many failure modes that can occur in electro-mechanical brakes. Other failure modes, such as the brake rotors wear, faults in the EMAs mechanical and electrical components or issues in the EMAs sensors can occur, and have a direct effect on the progression of other failure modes. Looking ahead, the authors have planned to pursue the definition of a PHM scheme able to

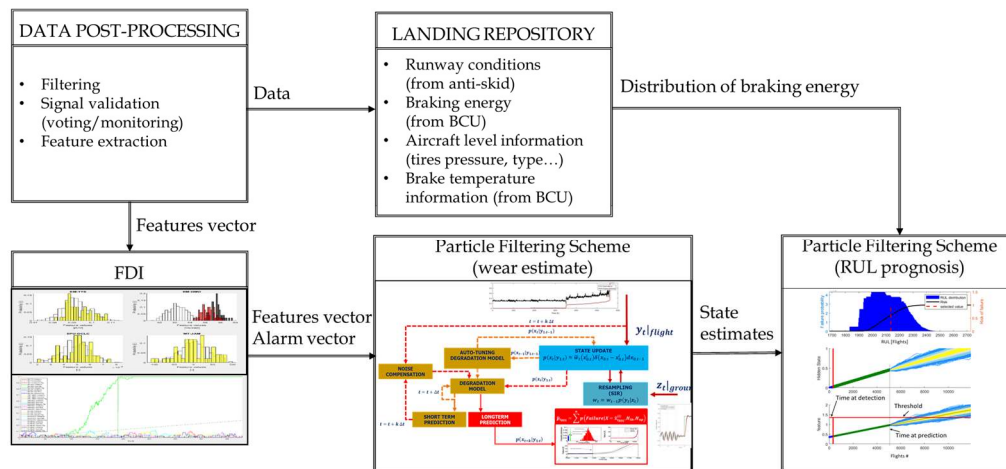


Figure 8. PHM Scheme.

define the expected RUL of the system including the possible cross-dependence between different failure modes. Particle-filtering techniques naturally lend themselves to this step, since their results are well-suited to data-fusion algorithms (Vachtsevanos et al., 2006). Moreover, being based on a physics-based description of the failure mode, the outcome of PF algorithms can be more easily interpreted from an engineering perspective and more easily included in digital-twin representations of the system under analysis.

Prognosis through particle filtering is achieved by performing two sequential steps, prediction and filtering. Prediction uses both the knowledge of the previous state estimate and the process model to generate the a priori estimate of the state probability density functions (pdfs) for the next time instant,

$$\begin{aligned} & p(x_{0:t}|y_{1:t-1}) \\ &= \int p(x_t|y_{t-1})p(x_{0:t-1}|y_{1:t-1}) dx_{0:t-1} \end{aligned} \quad (10)$$

This expression usually does not have an analytical solution, requiring Sequential Monte Carlo algorithms to be solved in real-time with efficient sampling strategies (Roemer et al., 2011). Particle filtering approximates the state pdf using samples or “particles” having associated discrete probability masses (often called “weights”) as,

$$p(x_t|y_{1:t}) \approx \tilde{w}_t(x_{0:t}^i)\delta(x_{0:t} - x_{0:t}^i)dx_{0:t-1} \quad (11)$$

where $x_{0:t}^i$ is the state trajectory and $y_{1:t}$ are the measurements up to time t . The simplest implementation of this algorithm, the Sequential Importance Re-sampling (SIR) particle filter (Arulampalam et al., 2009), updates the weights using the likelihood of y_t as:

$$w_t = w_{t-1}p(y_t|x_t) \quad (12)$$

Although this traditional particle filtering technique has limitations, in particular with regards to the description of the distributions tails, and more advanced resampling schemes have been proposed (Acuña & Orchard, 2017), this technique was still deemed valid for a purely preliminary analysis. Long-term prediction of the fault evolution can be obtained by iterating the “prediction” stage, and are used to estimate the probability of failure in a system given a hazard zone that is defined via a probability density function with lower and upper bounds for the domain of the random variable, denoted as H_{lb} and H_{up} , respectively. Given the probability of failure, the RUL distribution for any given prediction can be computed along with the risk function (Acuña & Orchard, 2018). The declination of the particle filter employed in this paper is based on a physics-based degradation model and a process model describing the dependency between the worn-out thickness x of the brake pads and the selected features.

$$\begin{cases} x_{N+1} = K_{wear}(E_{brake_N}) + x_N + \omega(N) \\ y_{N+1} = f(x_{N+1}, \nu(N)) \end{cases} \quad (13)$$

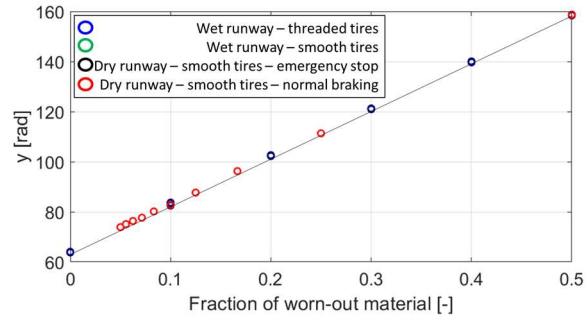


Figure 9. Dependency of the proposed feature on external factors and on degradation progression.

where K_{wear} is the wear constant, y is the feature and E_{brake_N} is the gross energy produced during the N^{th} landing. $\omega(N)$ and $\nu(N)$ are noises, estimated at each time step considering the probability distributions of the parameter and the accuracy of the process model through a certain number of previous steps.

The gross energy E_{brake_N} is estimated as follows, and provides an indication of an energy proportional to the terms of the modified Archard’s Equation provided in Equation 7, following the expression:

$$E_{brake_N} = r_{ebrake} \int_{t_0}^{t_{end}} \sum_{i=1}^4 F_i \omega_w dt \quad (14)$$

where F_i is the force exerted by each actuator and ω_w is the wheel angular frequency. The feature y is defined as the average angular position of the EMAs motor for which the measured force signal is significantly different from zero at the beginning of the braking procedure. Such data point is identified computing the rolling variance of the force signal and searching for the first point which rolling variance exceed 0.1. Such feature was successfully identified as the most promising in (De Martin, Jacazio, Parisi, et al., 2022) due to its high correlation with the degradation process. As shown in Figure 9, such feature is also not affected by variations in the operating conditions, nor by the braking procedure (emergency or normal). For each landing, the quantity E_{brake} is computed and memorized in a “landing repository”, where it is stored along with related aircraft-level information, such as the aircraft weight at landing, for future usage.

During the long-term prognosis, the “landing repository” data-base is used to build an array of possible future landings through random sampling. If an indication or prevision of the area in which the aircraft is going to typically operate is available, a planned feature is to further refine the sampling procedure to account for the most probable weather conditions. The prognostic algorithm is tested against 40 simulated fault-to-failure processes, where the wear of the brake pads evolves dynamically as a function of the system behavior and operating conditions (temperature, dynamic load, fluid pressure), with increasing number of particles N_p

(from 50 to 5000) and evaluated according to the traditional metrics provided by (Saxena et al., 2008), namely the Prognostic Horizon, evaluated as the first real RUL value for which the prognosis falls within a $\pm 20\%$ threshold of the real RUL, and the Relative Accuracy RA, defined as a function of the ground-truth value of the RUL (RUL_r) and its expected value RUL.

$$RA = 1 - \frac{|RUL_r - RUL|}{RUL_r} \quad (15)$$

An example of the prognostic output for the case of a is provided in Figure 10, where the system behavior is plotted against the number of simulated landing procedures N_L .

The behaviour of the particle filtering algorithm is investigated in two steps. At first considering the “filtering” performances, thus evaluating whether the system is able to correctly assess the severity of the on-going degradation, and secondly considering the long-term prognostic capabilities. Figure 11 depicts the behavior of the particle filter algorithm with respect to the simulated ground truth for the landing sequence already used for Figure 10, evidencing the particles distribution considering the estimated values assumed by the hidden state (the linear measure of the brake pad wear progression) and the selected feature. This information is given considering four equidistant prediction instances, with indication of the considered simulated landing.

It can be observed that the results of the particle-filtering routine are compatible with the simulated ground-truth in all of the shown cases, highlighting that the algorithm is able to coherently track the fault growth from the fault detection until imminent failure conditions. Figure 12 and Figure 13 describe the algorithm behavior against the simulated ground truth from a prognostic perspective. The estimated RUL distribution are coherent with the ground truth, and achieve convergence towards the simulated end-of-life.

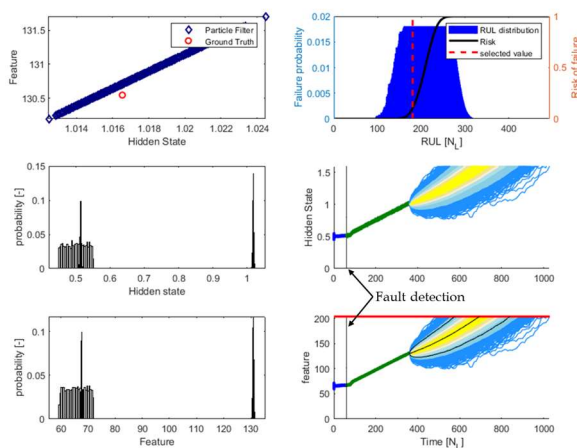


Figure 10. Prognostic performance against simulated dataset ($N_p = 5000$)

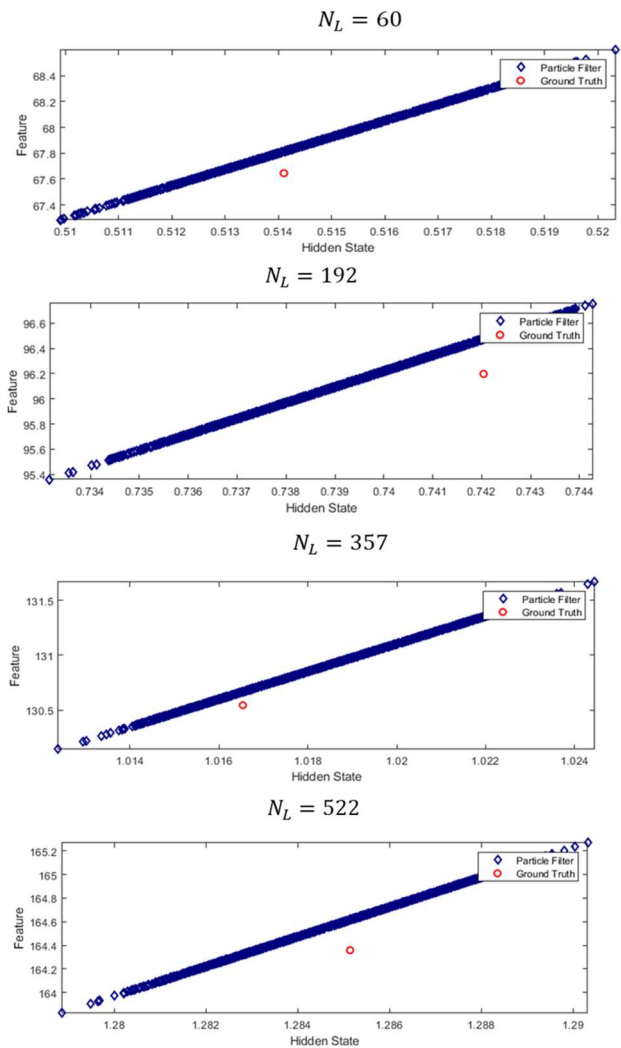


Figure 11. Comparison between PF and simulated ground-truth during the filtering stage ($N_p = 5000$)

In Figure 12, the RUL distribution at each considered prediction step is depicted along the selected value, corresponding to the RUL estimate with the highest probability of occurrence according to the algorithm. The “ground-truth” EOL, coming from simulation data set, is also provided. Results shows that the real EOL always falls within the prediction distribution, in the near proximity of values of risk of failure equal to 1. Although providing only anecdotal evidence – a more rigorous approach would be to compare the predicted RUL distribution against a real RUL distribution – this figure attests that the algorithm converges to the EOL in the analyzed case, providing then promising results.

This observation is confirmed by the $\alpha - \lambda$ diagram in Figure 13. The small deviation of the expected RUL with respect to the simulated ground-truth close to the EOL is expected to the prediction uncertainty increasing relatively to the RUL estimate.

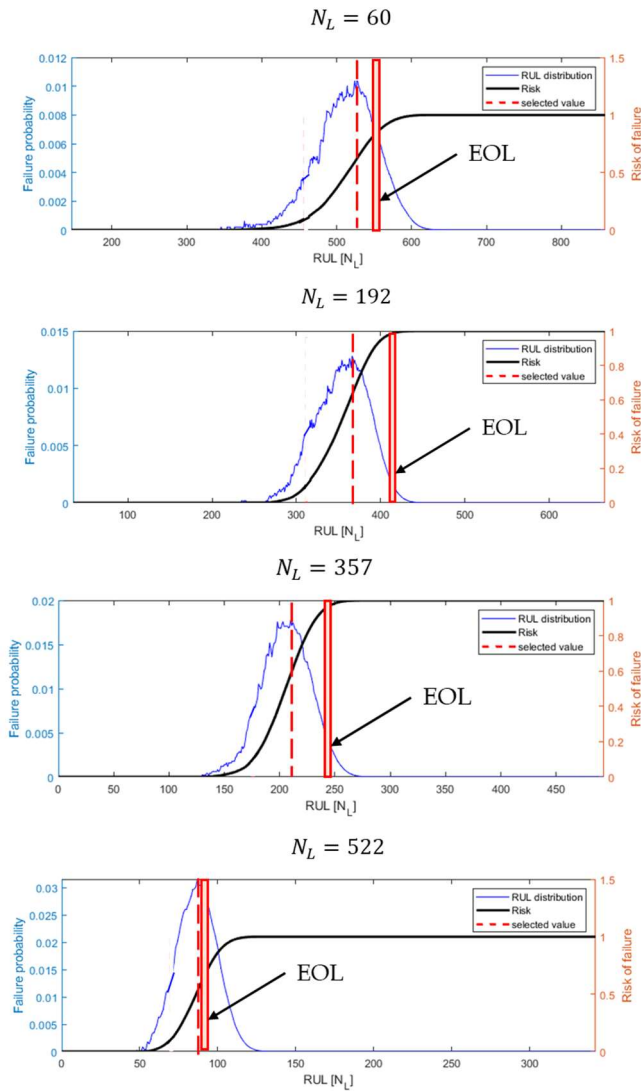


Figure 12. Comparison between estimated RULs at different prediction steps ($N_p = 5000$, $EOL = 600$ landings)

The prognostic performances of the algorithm are presented in terms of Relative Accuracy and Cumulative Relative Accuracy in Figure 14, where the results averaged over the 40 simulated landing sequences. It can be observed that the average Relative Accuracy remains well above the 80% threshold, while scoring high marks in CRA as well. Finally, the algorithm is evaluated considering its elapsed time, to verify whether it is suitable for on-board or on-line deployment. Results were obtained on a DELL Precision 3660 workstation with Intel Core i9-4.2 GHz and 64GB of DDR-4 RAM. Results are coherent with a possible real-time usage of the algorithm, although out of scope for the current project.

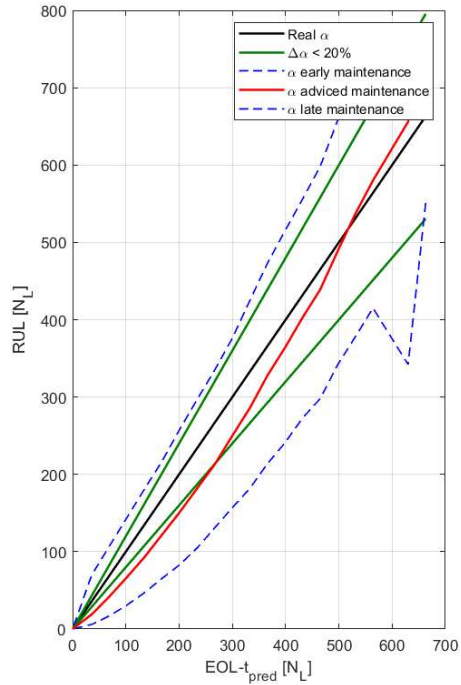


Figure 13. Dimensional $\alpha - \lambda$ diagram

6. PHM IMPLEMENTATION AND TEST PLAN

Given the intermittent nature of the E-Brake operations, PHM algorithms are expected to be run offline, without the need to suffice restrictive computational constraints to achieve a real-time identification of the fault occurrence or progression. After each landing data are collected and analyzed. These same considerations are carried to the technological demonstrator, which is thought to monitor the E-Brake health status considering the results coming after each test.

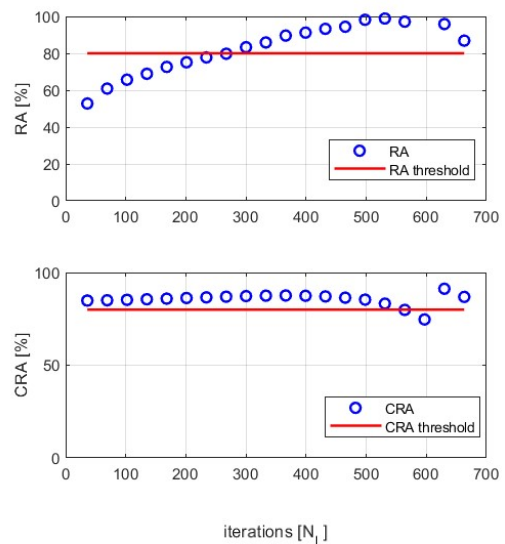


Figure 14. Prognostic performances (RA, CRA)

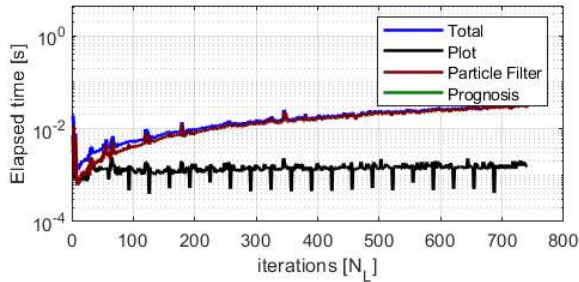


Figure 15. Algorithm elapsed time

The test plan is designed to verify and validate the most critical aspects of the presented work, namely the high-fidelity model employed to generate the synthetic database used to prepare the PHM activities and the wear model itself. Similarly, it is necessary to stress the PHM algorithm to check for false alarms and evaluate the performance of the prognostic output.

For these reasons the test plan includes:

- Registration of the qualification tests, including the simulated landing and the aborted take-off to evaluate the model behavior, considering different aircraft mass as detailed in Section 4.2.
- A number of consecutive landing simulations (at least 100), considering different aircraft weight and braking operation type (emergency, normal).
- The visual evaluation, after each landing, of the amount of worn thickness from the brake pads.

Since the test rig is not yet operational authors are not able to present the results of these activities, that will be hopefully the subject of further dissemination once the experimental steps are completed.

7. CONCLUSIONS

This paper presents the design of a novel technological demonstrator for PHM activities on a fully electrical landing gear and the preliminary design of a prognostic routine to forecast the wear in the pads of an electro-mechanical brake for a short-range aircraft. Since the test-rig is not yet operational, PHM activities have been tentatively proposed through a high-fidelity simulation model, iterating on the results of a previously published study. Such model, presented in the paper, is based on well-known equations, and translated into a state-of-the-art dynamic simulation engine. The PHM scheme is based on equations strictly correlated with the physics of the investigated degradation, and leverages the previous knowledge of the system usage to forecast the long-term estimate of the brake pads RUL. Early results are encouraging, but experimental support is needed to validate the findings of the simulation activities.

Further work will include the description and analysis of the effects of disks wear and the definition of health monitoring

schemes to detect and prognose other prominent failure modes potentially affecting electrical brakes.

REFERENCES

- Acuña, D. E., & Orchard, M. E. (2017). Particle-filtering-based failure prognosis via sigma-points: Application to Lithium-Ion battery State-of-Charge monitoring. *Mechanical Systems and Signal Processing*. <https://doi.org/10.1016/j.ymssp.2016.08.029>
- Acuña, D. E., & Orchard, M. E. (2018). A theoretically rigorous approach to failure prognosis. *Proceedings of the 10th Annual Conference of the Prognostics and Health Management Society 2018 (PHM18), Philadelphia, PA, September 24-27*.
- Arulampalam, M. S., Maskell, S., Gordon, N., & Clapp, T. (2009). A Tutorial on Particle Filters for Online Nonlinear/NonGaussian Bayesian Tracking. In *Bayesian Bounds for Parameter Estimation and Nonlinear Filtering/Tracking*. IEEE. <https://doi.org/10.1109/9780470544198.ch73>
- Bertolino, A. C., De Martin, A., Jacazio, G., & Sorli, M. (2023). Sizing and control system definition of an intelligent facility for qualification tests and prognostic research activities for electrical landing gear systems. *Materials Research Proceedings*, 26, 219–224. <https://doi.org/10.21741/9781644902431-36>
- Carbone, G., & Putignano, C. (2013). A novel methodology to predict sliding and rolling friction of viscoelastic materials: Theory and experiments. *Journal of the Mechanics and Physics of Solids*, 61(8), 1822–1834. <https://doi.org/10.1016/j.jmps.2013.03.005>
- De Martin, A., Jacazio, G., Parisi, V., & Sorli, M. (2022). Prognosis of Wear Progression in Electrical Brakes for Aeronautical Applications. *PHM Society European Conference*, 7(1), 329–337. <https://doi.org/10.36001/phme.2022.v7i1.3353>
- De Martin, A., Jacazio, G., Ruffinatto, A., & Sorli, M. (2022). A Novel Hydraulic Solution to Simulate Inertial Forces on a Landing Gear Qualification Test Rig. *Proceedings of the ASME/BATH Symposium on Fluid Power and Motion Control, FPMC2022*, 1–9.
- De Martin, A., Jacazio, G., & Sorli, M. (2022). Simulation of Runway Irregularities in a Novel Test Rig for Fully Electrical Landing Gear Systems. *Aerospace*, 9(2), 114. <https://doi.org/10.3390/aerospace9020114>
- Giannella, V., Baglivo, G., Giordano, R., Sepe, R., & Citarella, R. (2022). Structural FEM Analyses of a Landing Gear Testing Machine. *Metals*, 12(6). <https://doi.org/10.3390/met12060937>
- Grosso, L. A., De Martin, A., Jacazio, G., & Sorli, M. (2020). Development of data-driven PHM solutions for robot hemming in automotive production lines. *International Journal of Prognostics and Health Management*, 11, 1–13.

- M. Burckhardt. (1993). Radschlupf-Regelsysteme. *Fahrwerktechnik: Würzburg: Vogel Verlag.*
- Mohan, N., Undeland T.M., & Robbins, W. P. (2005). *Power Electronics* (3rd ed.). John Wiley and Sons, Inc.
- Oikonomou, A., Eleftheroglou, N., Freeman, F., Loutas, T., & Zarouchas, D. (2022). Remaining Useful Life Prognosis of Aircraft Brakes. *International Journal of Prognostics and Health Management*, 13(1), 1–11.
- Olesiak, Z., Pyryev, Y., & Yevtushenko, A. (1997). Determination of temperature and wear during braking. *Wear*, 210(1–2), 120–126. [https://doi.org/10.1016/S0043-1648\(97\)00086-0](https://doi.org/10.1016/S0043-1648(97)00086-0)
- Orchard, M. E., & Vachtsevanos, G. J. (2009). A particle-filtering approach for on-line fault diagnosis and failure prognosis. *Transactions of the Institute of Measurement and Control*. <https://doi.org/10.1177/0142331208092026>
- Ramesh, G., Garza, P., & Perinpanayagam, S. (2021). Digital simulation and identification of faults with neural network reasoners in brushed actuators employed in an e-brake system. *Applied Sciences (Switzerland)*, 11(19). <https://doi.org/10.3390/app11199171>
- Roemer, M. J., Byington, C. S., Kacprzyński, G. J., Vachtsevanos, G., & Goebel, K. (2011). Prognostics. In *System Health Management: With Aerospace Applications*. <https://doi.org/10.1002/9781119994053.ch17>
- Saxena, A., Celaya, J., Balaban, E., Goebel, K., Saha, B., Saha, S., & Schwabacher, M. (2008). Metrics for evaluating performance of prognostic techniques. *2008 International Conference on Prognostics and Health Management*, 1–17. <https://doi.org/10.1109/PHM.2008.4711436>
- Vachtsevanos, G., Lewis, F., Roemer, M., Hess, A., & Wu, B. (2006). Intelligent Fault Diagnosis and Prognosis for Engineering Systems. In *Intelligent Fault Diagnosis and Prognosis for Engineering Systems*. John Wiley & Sons, Inc. <https://doi.org/10.1002/9780470117842>
- Yevtushenko, A., Kuciej, M., & Topczewska, K. (2017). Analytical model for investigation of the effect of friction power on temperature in the disk brake. *Advances in Mechanical Engineering*, 9(12), 1–12. <https://doi.org/10.1177/1687814017744095>